

Lattice dynamics of quasi-two-dimensional CdSe nanoplatelets and their Raman and infrared spectra

Alexander I. Lebedev*

Physics Department, Moscow State University, 119991 Moscow, Russia

(Received 17 July 2017; revised manuscript received 19 October 2017; published 27 November 2017)

Phonon spectra of CdSe nanoplatelets (2–6 ML) with the zinc-blende structure were calculated from first principles within the density-functional theory. It turned out that the Lamb modes in nanoplatelets are in fact optical rather than acoustic vibrations. Phonon spectra of the nanoplatelets show the appearance of a large number of low-frequency modes inherited from TA phonons in bulk CdSe. Calculations of the Raman spectra indicate a need to revise the interpretation of available experimental data. The largest contribution to the Raman spectra is provided by the quasi-Lamb modes with the A_1 symmetry. The B_2 modes whose frequencies depend on the environment of nanoplatelets and whose properties are closest to the properties of LO phonons explain the results obtained in the “nanoparticle-on-mirror” geometry. The features in Raman spectra previously attributed to surface optical (SO) modes should be interpreted as a manifestation of lower-order quasi-Lamb A_1 modes. Calculations of the infrared spectra find, in addition to the TO phonon line, the appearance of intense lines from surface modes originating from terminating F(Cl) atoms on the surface of nanoplatelets and true SO modes.

DOI: [10.1103/PhysRevB.96.184306](https://doi.org/10.1103/PhysRevB.96.184306)

I. INTRODUCTION

Vibrational spectroscopy is one of the most important methods for studying materials. The lattice dynamics determines such physical properties of solids as elastic moduli, sound velocity, heat capacity, thermal expansion, thermal conductivity, and infrared absorption. In addition, the phenomena associated with the electron-phonon interaction determine the mobility of carriers in semiconductors and the changes in their electronic structure and optical spectra with temperature.

To determine the vibration frequencies, infrared (IR) and Raman spectroscopy as well as inelastic neutron scattering are used. Since the vibration frequencies are very sensitive to the local chemical environment and the structure of materials, the measurement of these frequencies and their comparison with the calculated frequencies and atomic displacement patterns can give detailed information on atomic and electronic structure of materials.

The physical properties of semiconductor nanoplatelets are qualitatively different from those of bulk materials. In addition to the well-studied quantum size effects, this also applies to the phonon spectra of these quasi-two-dimensional systems. As was shown in a classical paper of Lamb [1], in the spectra of acoustic vibrations of thin plates, along with two acoustic modes with in-plane polarization, a new type of acoustic vibrations arises, in which the atoms are displaced in the out-of-plane direction and for which the quadratic dispersion law is characteristic ($\omega \sim q^2$, where q is the in-plane component of wave vector). The peculiarities of optical vibrations in thin plates were discussed in Refs. [2,3].

The objects of this study are quasi-two-dimensional CdSe nanoplatelets with the zinc-blende (ZB) structure. Like other cadmium chalcogenides, cadmium selenide is currently an object of considerable interest due to unique optical properties which are observed in nanoobjects of various shapes and are controlled by the size effect and by creating of

heterostructures. In particular, CdSe colloidal nanoplatelets with a thickness of few monolayers [4,5] are characterized by atomically flat surfaces. Very homogeneous thickness of the nanoplatelets results in very narrow luminescence bands. The giant oscillator strength of the exciton transitions in them [6] results in very short luminescence decay times (hundreds of picoseconds) [7,8] and high absorption coefficients, which are much higher than those for quantum dots [9]. Record narrow absorption and emission bands resulting from the thickness-dependent exciton transitions make them promising materials for the development of new types of light-emitting devices [10–12], lasers [13–15], photodetectors [16], and other optoelectronic devices.

The literature data on Raman and IR spectra of CdSe nanoplatelets are not too numerous [17–21]. The main strong peak in the Raman spectra is explained by the light scattering by LO phonons whose frequency varies with a change in the nanoplatelet thickness as a result of the spatial confinement of the phonons. The weak features observed on the low-energy side of this peak are explained by surface optical (SO) phonons [17,18,21]. In Refs. [17,18], the thickness dependence of the frequencies of LO and SO modes was studied. Under nonresonant excitation, the position of Raman peaks did not depend on the thickness. Under resonant excitation (the excitation energy was close to the energy of the exciton transition), the energy of the peaks decreased noticeably (by 2.5–7.5 cm^{-1}) and their width slightly increased with decreasing nanoplatelets thickness. This difference in behavior was explained by preferential light scattering by $\text{LO}(x)$ phonons (in the case of nonresonant excitation) or by confined $\text{LO}(z)$ modes (in the case of resonant excitation). In Ref. [19], Raman spectra from individual nanoplatelets were obtained using the surface-enhanced Raman scattering (SERS) in the “nanoparticle-on-mirror” (NPOM) geometry. These spectra consisted of two overlapping lines, one of which, attributed to the $\text{LO}(z)$ phonon, appeared at an energy by 7–10 cm^{-1} lower than the energy of the other line whose position was close to the energy of the line measured in standard geometry and ascribed to $\text{LO}(x)$ phonon. In Ref. [20],

*swan@scon155.phys.msu.ru

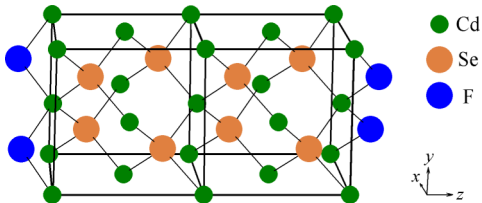


FIG. 1. The structure of CdSe nanoplatelet with a thickness of 4 ML.

the low-frequency lines associated with intrinsic mechanical vibrations of nanoplatelets were detected in Raman spectra. The frequencies of these vibrations, however, were 40–50% below the calculated ones. This discrepancy was explained by the effect of heavy molecules of oleic acid located on the surfaces of nanoplatelets on the vibration frequency. In Ref. [21], Raman spectra of CdSe nanoplatelets were measured at low temperature (35 K) and at different excitation energies. These measurements confirmed the appreciable long-wave shift and broadening of the main line in the spectra under resonant excitation and revealed a complicated structure of the SO mode. In addition, in this work infrared reflection spectra of CdSe nanoplatelets were obtained, and the features associated with LO and TO phonons were observed.

In this work, the first-principles calculations of the lattice dynamics of CdSe nanoplatelets are supplemented by modeling their Raman and infrared absorption spectra to better understand what information can be obtained from these optical studies. Based on the comparison of the results of calculations with available experimental data, an interpretation of these data is proposed.

II. CALCULATION DETAILS

All calculations in this paper were performed within the density functional theory using the ABINIT software package. In the calculations, the local density approximation (LDA), plane-wave basis, and norm-conserving pseudopotentials were used. The cutoff energy was 30 Ha (816 eV), the integration over the Brillouin zone for the starting FCC lattice was carried out on a $8 \times 8 \times 8$ Monkhorst-Pack mesh. The relaxation of the unit cell parameters and atomic positions was carried out until the Hellmann-Feynman forces acting on the atoms became less than 5×10^{-6} Ha/Bohr (0.25 meV/Å).

In accordance with modern concepts of the structure of CdSe nanoplatelets with the ZB structure, the studied nanoplatelets were [001]-oriented slabs, both surfaces of which ended in cadmium atoms (Fig. 1). Since the nanoplatelets contain one excess plane of Cd atoms, the extra charge of 5s electrons introduced by these atoms requires electrical compensation. In this paper, we considered the simplest method of charge compensation using the surface F or Cl atoms. As shown in Ref. [22], energetically the most favorable position of these surface atoms are the bridge positions in which the halogen atoms enter the positions of the missing selenium atoms in the ZB structure (Fig. 1). Modeling of nanoplatelets was carried out using supercells to which a vacuum gap of 20 Å was added to isolate nanoplatelets from each other. The symmetry of such a supercell is

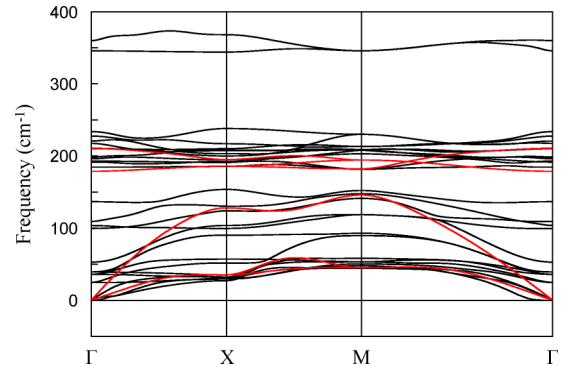


FIG. 2. Phonon spectra for CdSe nanoplatelet with a thickness of 3 ML terminated with F atoms (black lines) and bulk CdSe (red lines).

described by $P\bar{4}m2$ space group. The thickness of nanoplatelets varied from 2 to 6 monolayers (ML). When modeling the nanoplatelets, $8 \times 8 \times 2$ Monkhorst-Pack meshes were used for the integration over the Brillouin zone. All the results presented below were obtained on fully relaxed structures with stress-free surfaces.

Calculations of the phonon frequencies at the center and high-symmetry points at the boundary of the Brillouin zone, the Born effective charges $Z_{\alpha\beta}^*$, the high-frequency dielectric constant $\epsilon_{\alpha\beta}^\infty$, the oscillator strengths $S_{k,\alpha\beta}$, and the Raman susceptibility tensor were performed using the formulas obtained from the density-functional perturbation theory [23,24]. Raman spectra of randomly oriented nanoplatelets were obtained using the formulas given in Ref. [25] by calculating the rotational invariants of the Raman tensors and the Bose factors for 300 K. Infrared spectra (imaginary part of the complex dielectric constant) were calculated using the formula $\epsilon_{\alpha\beta}^\infty(\omega) = \epsilon_{\alpha\beta}^\infty + (4\pi/\Omega) \sum_k S_{k,\alpha\beta} / [\omega_k^2 - \omega^2 - i\gamma\omega]$, where the sum runs over all modes k , ω_k is the frequency of the k th mode at the Γ point, and Ω is the unit cell volume. The calculated spectra were then averaged in order to obtain spectra of randomly oriented nanoplatelets. Dispersion curves in the phonon spectrum were calculated using the anaddb program (a part of the ABINIT package) by interpolating the results of exact calculations of phonon frequencies on a 8×8 mesh of wave vectors (15 irreducible points in the Brillouin zone).

III. PHONON SPECTRA OF THE NANOPATELETS

The phonon spectrum of a typical quasi-two-dimensional CdSe nanoplatelet with the ZB structure terminated by F atoms is shown in Fig. 2. In the figure we present only the dispersion curves for the square (two-dimensional) Brillouin zone because, as was confirmed by calculations on supercells, the dispersion of the phonon modes in the out-of-plane direction is absent.

We now discuss the character of phonon modes at the Γ point for a typical nanoplatelet with a thickness of 3 ML (nine atoms in the unit cell). After the removal of three acoustic modes corresponding to the translation of the nanoplatelet in three directions, 24 optical modes remain at the Γ point. In 16 of them, the atomic displacements occur in the plane of the nanoplatelet (xy), and in the other eight modes the

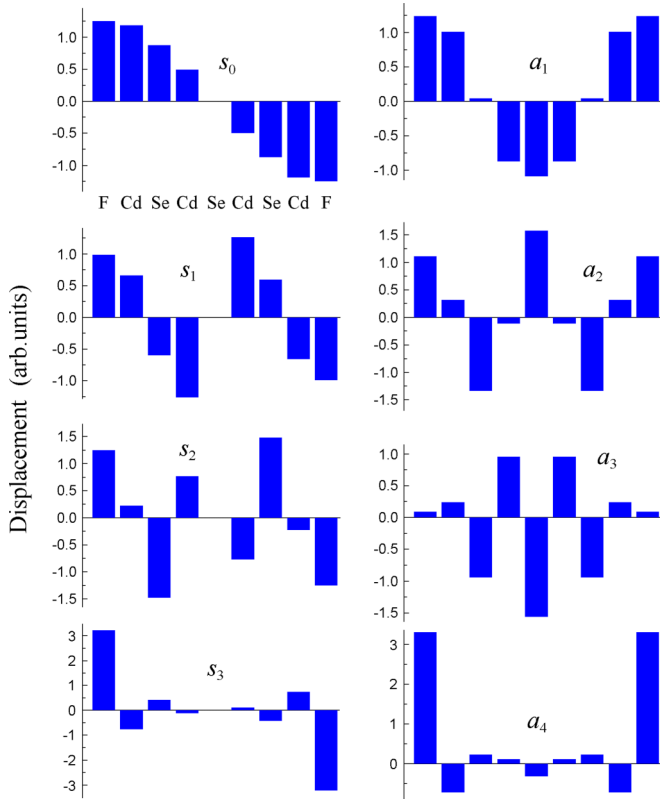


FIG. 3. The atomic displacement patterns of quasi-Lamb modes at the Γ point for CdSe nanoplatelet with a thickness of 3 ML terminated with F atoms. The modes and their frequencies: s_0 —53 cm^{-1} , a_1 —100 cm^{-1} , s_1 —137 cm^{-1} , a_2 —196 cm^{-1} , s_2 —211 cm^{-1} , a_3 —221 cm^{-1} , s_3 —234 cm^{-1} , a_4 —228 cm^{-1} . The direction of the displacements is out-of-plane.

displacements are out-of-plane (z direction). By the character of the displacement patterns, the latter eight modes are similar to the Lamb modes (Fig. 3). The symmetric Lamb modes s_i [26] (symmetry A_1) have zero Born effective charge ($Z^* = 0$), whereas the antisymmetric Lamb modes a_i (symmetry B_2) are characterized by a small effective charge ($Z_{zz}^* = 0.070$ – 1.039), which indicates the appearance of polarization that accompanies vibrations. The appearance of the polarization is not related to the piezoelectric properties of CdSe since it cannot arise from the strain of the sample along the $[001]$ direction. The polarization arises as a result of the displacement of atomic planes carrying a small ionic charge (the chemical bond in CdSe has a mixed covalent-ionic character). Because of the appearance of a long-range dipole-dipole interaction, the corresponding vibrational modes should be interpreted as *optical* rather than acoustic vibrations [27]. In what follows we shall refer to them as quasi-Lamb modes. This feature of the Lamb waves can also be characteristic of nanoplatelets made of other dielectric materials.

In order to clarify the relationship between quasi-Lamb modes and normal modes in bulk CdSe, we performed the mode projection analysis by expanding the eigenvectors of the quasi-Lamb modes in an orthogonal basis of normal modes of bulk CdSe. This technique was first used for studying the vibrational spectra of CdSe quantum dots in Ref. [28].

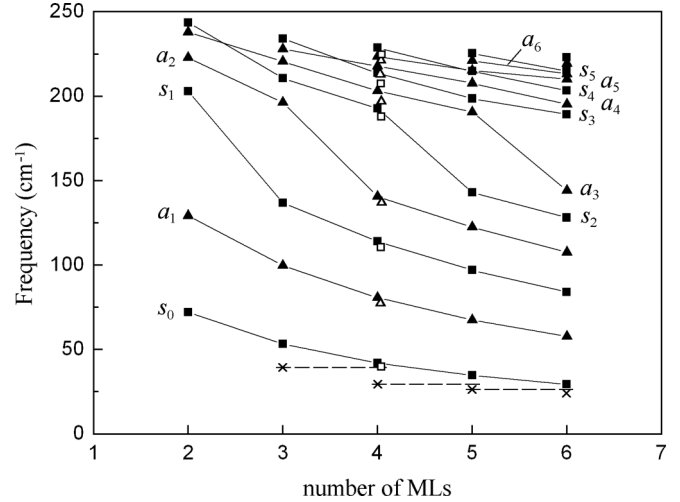


FIG. 4. Evolution of the frequencies of quasi-Lamb modes with a change in the thickness of CdSe nanoplatelets terminated by F atoms from 2 to 6 ML. Open symbols show the frequencies for a nanoplatelet terminated by Cl atoms. Crosses are the experimental frequencies taken from Ref. [20].

In contrast to quantum dots, the vibrational spectra of CdSe nanoplatelets are described by good quantum numbers (q_x , q_y , indexes of the s_i and a_i Lamb modes), and so the z component of wave vector q_z is the only parameter which can be considered as an expansion parameter. The obtained results are presented in the Supplemental Material [29]. Due to the symmetry of nanoplatelets, the LA and LO(z) modes are the only modes which contribute to the A_1 and B_2 quasi-Lamb modes. The largest contribution to the low-order A_1 modes comes from LA phonons with $q_z \neq 0$, whereas the largest contribution to the high-order A_1 modes is from LO(z) phonons with $q_z \neq 0$. The largest contribution to the B_2 mode a_i whose index i is equal to the number of MLs in the nanoplatelet is provided by $q = 0$ LO phonon of bulk CdSe (this mode has the highest Z_{zz}^* value). The largest contribution to other B_2 modes are from the LA (low-order modes) or LO(z) (high-order modes) phonons with $q_z \neq 0$.

The frequencies of quasi-Lamb modes at the Γ point as a function of the thickness of nanoplatelets are shown in Fig. 4. The figure does not include results for the flexural a_0 mode whose frequency is always zero at $q = 0$. It is seen that the frequencies of high-order quasi-Lamb modes are grouped near the frequency of LO phonon in bulk CdSe (210 cm^{-1} in our calculations). When increasing the nanoplatelet thickness, the lower-order modes “split off” from this group, and their frequencies rapidly decrease. According to the mode projection analysis, the largest contribution to the modes that are grouped around 210 cm^{-1} is made by LO phonons. The fact that the frequencies of these modes exceed the frequency of TO phonon in bulk CdSe (179 cm^{-1} in our calculations) indicates the existence of the dipole-dipole interaction in both A_1 and B_2 quasi-Lamb modes in the nanoplatelets. The replacement of the surface F atom by Cl results in a small (2–6 cm^{-1}) lowering of the frequencies of all quasi-Lamb modes (Fig. 4).

The results shown in Fig. 4 can be used to determine the thickness of nanoplatelets. As the frequencies of quasi-Lamb

modes depend on the mass of the surface atoms, and in the experimental nanoplatelets the surface atom is usually oxygen whose mass is close to that of fluorine, then Fig. 4 can be directly used to solve this problem. With this aim, we superimposed the experimental data from Ref. [20] on our calculated curves. As in Ref. [20], the observed vibration frequencies are somewhat lower than the calculated ones, but if one assumes that the nanoplatelet is actually by one monolayer thicker [30], the agreement becomes good. As for the model used in Ref. [20], one should note that a model with an additional mass located on the surface of a nanoplatelet is not entirely adequate to the experiment since the thickness of the oleic acid layer on the surface of the nanoplatelet is comparable with the nanoplatelet thickness. Taking into account the difference between the sound velocities in CdSe and oleic acid, the model [31] of a plate covered with a medium whose acoustic wave impedance is substantially (about an order of magnitude) smaller than that of CdSe seems to be more adequate.

As was mentioned in Sec. I, one of the acoustic modes (a_0) in the vibrational spectra of thin plates is purely flexural, and for small q its dispersion law is $\omega \sim q^2$. Such a dispersion law can indeed be seen in the phonon spectra of nanoplatelets in Fig. 2 in the vicinity of the Γ point.

All optical modes with the E symmetry and in-plane atomic displacements are characterized by nonzero effective charge. When analyzing these modes, we see a large number of modes that are absent in bulk CdSe and appear in the phonon spectra of nanoplatelets in the frequency range 25–90 cm^{-1} (Fig. 2). In order to understand their origin, we performed the mode projection analysis of these modes (see the Supplemental Material [29]). Due to the symmetry of nanoplatelets, the TA and TO phonons are the only modes which contribute to the E modes. It turned out that in a nanoplatelet with a thickness of n MLs, there are n modes with a dominant contribution from TA phonons of bulk CdSe with $q_z \neq 0$, and the remaining modes have a dominant contribution from TO phonons.

The characteristic “doubling” of atomic displacements, which is observed for all acousticlike E modes on the left panel in Fig. 5, and the fact that the eigenvectors of these modes are directed along the $[110]$ and $[1\bar{1}0]$ axes, support their relationship with TA phonons in bulk CdSe. Indeed, when the atoms in the (001) planes in the ZB structure are displaced along the indicated directions, two types of stresses of interatomic bonds arise in adjacent planes: one generating elongation and shortening of bonds and the other changing the angles between them without changing their lengths. Since the energy cost necessary to change the angles between the bonds is much less than that required to change their lengths, we immediately get a set of two strongly different local “shear moduli”. The “doubling” of atomic displacements is a consequence of this difference: Atomic layers bound by stronger bonds experience smaller relative displacement. These pairs of atomic layers are bound with other pairs by much weaker bending bonds, which result in the low-frequency acousticlike modes.

Next $n - 1$ E modes are the modes with frequencies in the range 181–194 cm^{-1} . The mode projection analysis shows that only the lowest of these modes has a dominant contribution

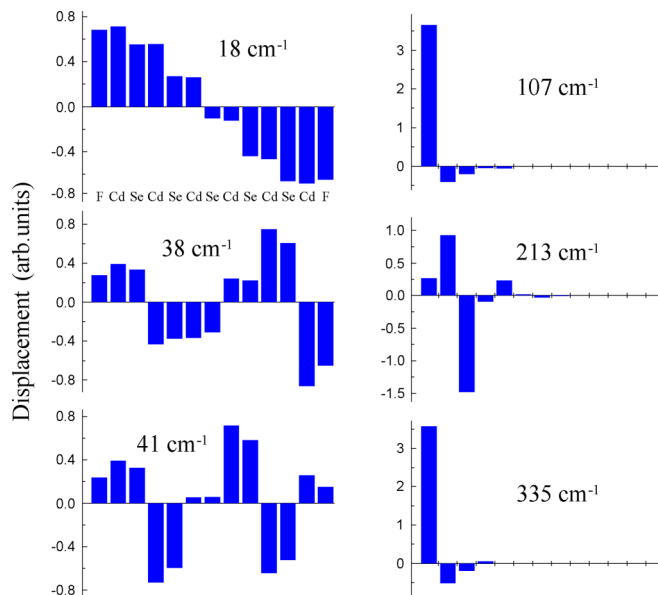


FIG. 5. Eigenvectors of several vibrational modes of the E symmetry for CdSe nanoplatelet with a thickness of 5 ML terminated with F atoms. The left panel shows modes with frequencies of 18 cm^{-1} , 38 cm^{-1} , and 41 cm^{-1} . The right panel shows surface vibrational modes with frequencies of 107 cm^{-1} , 213 cm^{-1} , and 335 cm^{-1} . The atomic displacements are in the plane of the nanoplatelet.

from $q = 0$ TO phonon of bulk CdSe, whereas the modes with higher energies result from TO phonons with $q_z \neq 0$.

Finally, the last group of the E modes (right panel in Fig. 5) can be interpreted as surface modes: The amplitude of atomic vibrations decays very rapidly when moving deep into the nanoplatelet. The maximum displacement is experienced by surface F atoms or atoms of the first monolayer. The mode projection analysis shows that they have a roughly equal contributions from all TO phonons in the whole Brillouin zone. Modes with frequencies of 107 and 335 cm^{-1} , which have very similar displacement patterns, differ in frequency by more than three times. In the first of these modes, the displacements of F occur perpendicularly to their chemical bonds with Cd (the bending mode), whereas in the second of them the displacement of fluorine causes an elongation of one and shortening of the other of these bonds (the stretching mode). This explains the difference in their frequencies. The frequencies of these two modes significantly decrease (by 30–50%) when replacing F atoms by Cl atoms.

As concerns the mode with a frequency of 213 cm^{-1} , we associate it with a so-called surface optical (SO) mode. According to the theory [3], for a thin slab, the frequency of this mode should exactly coincide with the frequency of bulk TO phonon [32]. Our calculations do indeed find such a surface E mode (Fig. 5). In the nanoplatelet with a thickness of n MLs, this mode always appears as the highest-energy optical E mode whose eigenvector qualitatively differs from that of other optical E modes. There are two reasons for the observed upward shift of the frequency of the SO mode as compared to that of TO phonon: (1) according to the mode projection analysis, TO phonons from the whole Brillouin zone contribute almost equally to this mode; (2) there is a large contribution

from the terminating F atom into this mode (the replacement of F by Cl decreases the SO mode frequency by 13–15 cm^{-1}). In contrast to quantum dots [28], in nanoplatelets the SO mode has not a mixed LO+TO character, but is a purely transverse mode.

We note that a similar picture with strong displacements of surface F atoms typical of surface modes can be seen for two highest-frequency quasi-Lamb modes (s_3, a_4) in Fig. 3. In the mode projection analysis, these modes display a behavior that is different from the behavior of both F surface modes and other quasi-Lamb modes. On the other hand, the arguments against their surface character are: (1) the frequencies of these modes exhibit very little change (2–4 cm^{-1}) upon replacing the terminating F atoms by Cl atoms and (2) a sufficiently high displacement amplitude is retained in the bulk of a nanoplatelet even for the thickest of them. Nevertheless, we tend to classify these modes as surface modes, whose z displacements are strongly coupled with the LO-type displacements of atoms in the bulk of the nanoplatelet due to the long-range dipole-dipole interaction. This assumption let us propose the following simple picture that describes the phonon spectrum of all nanoplatelets.

The unit cell of a CdSe nanoplatelet with a thickness of n MLs contains $2n + 3$ atoms and produces $3(2n + 3)$ vibrational modes. Three of them, the flexural a_0 mode, one LA, and one TA phonons polarized in the xy plane are acoustic ones, the other $6(n + 1)$ modes are optical. The first $6n$ modes are produced by n CdSe monolayers. These are: n symmetric quasi-Lamb s_i modes ($i = 0 \dots n - 1$), n antisymmetric a_i modes ($i = 1 \dots n$), and $2n$ doubly degenerate optical E modes, half of which are acousticlike, and the other half are opticlike (the TO-like mode with the highest energy produces the so-called SO mode). The remaining six modes, two doubly-degenerate surface E modes, s_n , and a_{n+1} modes, are associated with vibrations of two terminating F(Cl) atoms.

IV. INTERPRETATION OF RAMAN AND IR SPECTRA

The Raman spectra of CdSe nanoplatelets in the back-scattering geometry calculated for nonresonant excitation conditions are shown in Fig. 6. In modeling the spectra, we intentionally used a small parameter of the Lorentz broadening for a fine structure in the spectra could be seen; in the experiment, these details can be less visible because of stronger damping of the vibrations. It is seen that the largest contribution to the spectra is provided by the fully symmetric quasi-Lamb A_1 modes s_i and—to a much lesser degree—by the high-order B_2 modes a_i , which are analogs of the LO modes. The relative contribution of the B_2 modes to the Raman scattering weakens as the nanoplatelet thickness increases. From the modes with the E symmetry, a weak contribution to the Raman spectra is provided by the mode with the lowest frequency (asterisks in Fig. 6); the intensity of other E modes [including LO(x) mode] is by 1–2 orders of magnitude smaller. In spite of a large spread in positions and intensities of individual lines near 210 cm^{-1} , the center of gravity of these lines is a rather smooth function of the nanoplatelet thickness. It locates slightly above the LO phonon frequency in bulk CdSe and slowly decreases with increasing nanoplatelet thickness [33].

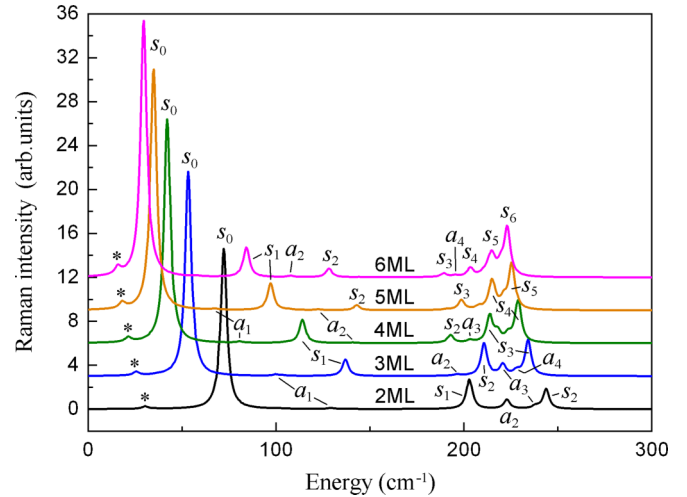


FIG. 6. Calculated Raman spectra for CdSe nanoplatelets with a thickness from 2 to 6 ML terminated with F atoms. The asterisks show the most intense of the E modes.

The difference in intensities of the A_1 and B_2 Raman lines results from the different symmetry of their corresponding Raman tensors,

$$\begin{pmatrix} \alpha & 0 & 0 \\ 0 & \alpha & 0 \\ 0 & 0 & \gamma \end{pmatrix} \text{ and } \begin{pmatrix} 0 & \beta & 0 \\ \beta & 0 & 0 \\ 0 & 0 & 0 \end{pmatrix}.$$

Since the α values are usually two times larger than the β values and $\gamma \approx 0.1\alpha$, the isotropic invariant produced by the first of these tensors results in a much higher intensity of Raman lines than the symmetric anisotropic invariant produced by the second tensor (for details see the Supplemental Material [29]).

The difference between the A_1 and B_2 modes is of fundamental character. Although both of these modes can be expanded in a series of normal modes of bulk CdSe, their properties are very different: Only one of polar B_2 modes transforms to the bulk polar LO phonon when increasing nanoplatelet thickness. The A_1 modes, which can be considered as standing waves formed from two LO phonons with $q_z \neq 0$, can appear only in the restricted geometry. The main feature of the A_1 mode—it is nonpolar and does not produce a long-range electric field—has no corresponding solution in bulk systems. So, the A_1 mode is a new type of vibration specific to quasi-two-dimensional structures. Breathing modes in quasi-0D systems and radial breathing modes in quasi-1D systems are other examples of such modes. Thus, our calculations do not confirm the commonly accepted interpretation of the main peak in Raman spectra of CdSe nanoplatelets as a manifestation of LO phonon.

The results of our calculations show that the explanation of the observed differences between nonresonant and resonant Raman spectra [17,18] may be incorrect, too. In order for two lines of approximately equal amplitude to appear in the resonant Raman spectrum, the intensity of the E mode should be increased by three orders of magnitude with respect to the intensity of the A_1 mode with close frequency, which seems unlikely. A more natural explanation is the change in the intensity of different A_1 modes, which form a fine structure

in the spectra, under resonant conditions. An experimental confirmation of the existence of the fine structure in Raman spectra is its observation in CdSe/CdS nanoheterostructures upon changing the excitation energy [21].

We now discuss the interpretation of weak features that are observed on the low-energy side of the main Raman peak and are explained by surface optical (SO) phonon. As was mentioned above, our calculations do indeed find such a surface E mode (mode with a frequency of 213 cm^{-1} in Fig. 5). This mode should obviously be observed in the IR absorption spectra (see below), but according to our calculations, in the Raman spectra its intensity is three orders of magnitude smaller than the intensity of the nearest strong line. This means that the features which have been explained by SO phonon have a different origin. We believe that these features actually result from other lines in the fine structure of the calculated Raman spectra, first of all from the fully symmetric quasi-Lamb A_1 modes of lower order. The fine structure of SO mode revealed in Ref. [21] supports this interpretation. Obviously, the peaks attributed to the combination LO+SO in Ref. [21] should be interpreted as a second-order scattering on the combination of the A_1 modes.

Long-wavelength shifts of Raman lines observed in the NPOM geometry [19], in our opinion, indicate the modes that, in finite-size systems, create an electric field outside the sample and therefore depend on the geometry of measurements and the dielectric constant of surrounding medium. Among the modes existing in CdSe nanoplatelets only the B_2 modes have such a property.

In order to verify the correctness of our reasoning, we calculated the mode frequencies in several nanoplatelets with the same positions of atoms, but with an increased thickness of the vacuum gap. It is obvious that the frequency of the B_2 modes, for which the electric field is nonzero outside the sample, should depend on the size of this gap because the electric field energy in the gap is proportional to its thickness. It turned out that upon an increase in the thickness of the vacuum gap by 6 \AA for the 3 ML nanoplatelet, the frequencies of only two modes changed more than 0.01 cm^{-1} : these were the B_2 modes—the a_3 mode (the frequency increment was 0.32 cm^{-1}) and the a_4 mode (the frequency increment was 1.29 cm^{-1}). These are the modes whose frequencies can change significantly when the environment of a nanoplatelet changes. For the 5 ML nanoplatelet, a noticeable increase in the frequency was also observed for two B_2 modes—the a_5 mode (the frequency increment was 1.17 cm^{-1}) and the a_6 mode (the frequency increment was 0.51 cm^{-1}) for the same increase in the thickness of the vacuum gap. Therefore, it is not surprising that when the gap in the NPOM geometry was reduced, a decrease in the frequency of the B_2 mode was observed [19]. The “plasmonic amplification” of the intensity of this mode in the NPOM geometry is the reason for the appearance of the second line in the Raman spectrum in addition to the A_1 line. Our interpretation of the observed changes in the spectra differs from that proposed in Ref. [19]. In addition, the authors are not correct when considering the B_2 modes inactive in the standard Raman geometry.

Calculations of the infrared absorption spectra (Fig. 7) show that the largest contribution to them is provided by the E mode with the highest effective charge and the displacement

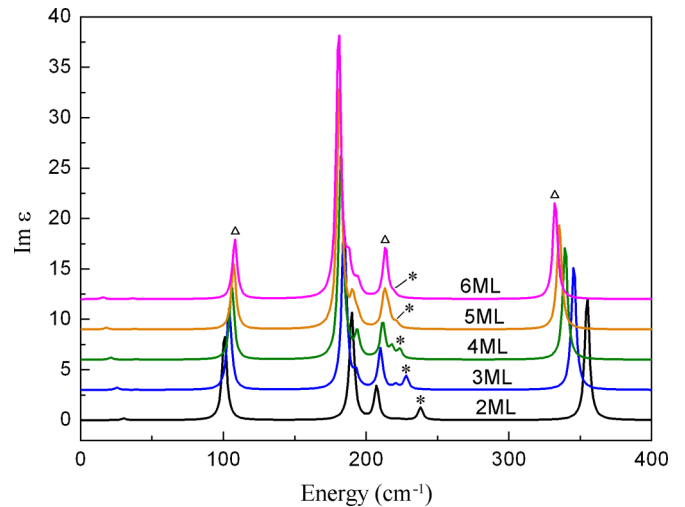


FIG. 7. Calculated infrared absorption spectra ($\text{Im } \epsilon$) for CdSe nanoplatelets with a thickness from 2 to 6 ML terminated with F atoms. Asterisks mark the B_2 modes; triangles mark the surface modes.

pattern closest to that of TO phonon in bulk CdSe. As the thickness of the nanoplatelet increases, the frequency of this mode tends to the frequency of TO phonon in bulk CdSe. On the high-energy side of this peak one can see a structure resulting from the E modes corresponding to TO phonons with $q_z \neq 0$. Three peaks of medium intensity (triangles in Fig. 7) are related to the surface modes whose eigenvectors are shown on the right panel in Fig. 5. The true SO mode, which was discussed above, can be clearly seen as a separate feature in the IR reflection spectra [21]. Finally, a very small contribution to the spectra is provided by the quasi-Lamb B_2 modes (asterisks in Fig. 7). Although the dipole moments arising from the latter vibrations are directed out-of-plane, we can observe them because nanoplatelets have a random orientation with respect to the direction of light propagation. In summary, we see that the IR spectra can provide important information on the TO-like modes and the surface vibrations in nanoplatelets.

Lastly, a comment about the phonon confinement model [34] should be added. This model can indeed be regarded as a way for estimating the shifts of LO and TO phonon frequencies in Raman spectra of nanostructured materials. However, the phonon confinement model is usually concentrated on the analysis of only these modes, whereas in this paper we have revealed much more complex behavior resulting in the appearance of vibrational modes which are missing in the phonon confinement model, but are observable in optical spectra. The frequencies of twenty-five Raman-active modes for the 6 ML CdSe nanoplatelet are compared with the phonon spectrum of bulk CdSe in Fig. 8. It is seen that the frequencies of these modes are qualitatively consistent with the frequencies of phonon modes of bulk CdSe taken at q_z vectors which provide the largest contribution to the eigenvector of the corresponding mode. Nevertheless, in some cases the frequencies can differ by $10\text{--}15\text{ cm}^{-1}$, as for the highest-energy mode which corresponds to the strongest line in the Raman spectrum. We note that both the phonon

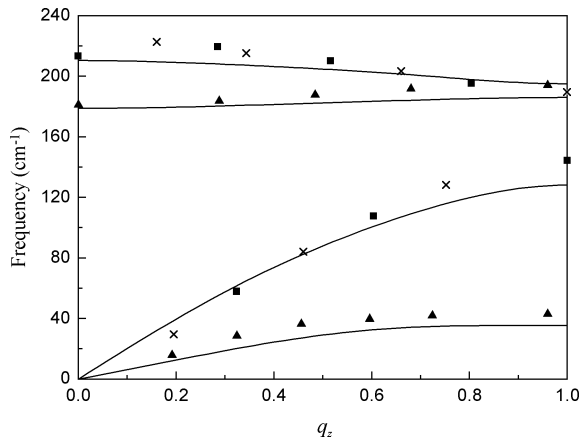


FIG. 8. Comparison between the frequencies of Raman-active modes for the 6 ML CdSe nanoplatelet and phonon spectrum of bulk CdSe. The q_z values are the wave vectors that make the largest contribution to the modes according to the mode projection analysis. Triangles: data for the E modes, squares: data for the B_2 modes, crosses: data for the A_1 modes.

dispersion curves and the mode frequencies presented in the figure were calculated using the same technique. The origin of this difference is that in our lattice dynamics calculations of nanoplatelets, we used relaxed structures and calculated the force constants from first principles individually for each atom, thus avoiding the question of how to define “the nanoplatelet thickness”. The difference between our approach and the phonon confinement model may be especially big when calculating Raman and IR spectra of nanoheterostructures, in which the thickness of the outer layer can be as small as 1 ML and where the phonon confinement model becomes inapplicable.

V. CONCLUSIONS

The first-principles calculations of the lattice dynamics of CdSe nanoplatelets have shown that the Lamb modes in them are in fact optical not acoustic vibrations. In the spectra of optical vibrations of nanoplatelets, there appears a large number of low-frequency modes inherited from TA phonons in bulk CdSe. Calculations of the Raman spectra show that the largest contribution to them is provided by the fully symmetric quasi-Lamb modes with the A_1 symmetry. Antisymmetric quasi-Lamb modes with the B_2 symmetry, whose frequencies depend on the environment of a nanoplatelet and whose properties are closest to the properties of LO phonons, enable to explain the results of Raman studies in the NPOM geometry. It is shown that weak lines in Raman spectra previously attributed to surface optical (SO) phonons should be interpreted as a manifestation of lower-order quasi-Lamb A_1 modes. Calculations of the infrared spectra find, in addition to the TO phonon line, the appearance of intense lines of surface modes originating from the atoms on the nanoplatelet surface and from true SO modes. The results obtained in this work can be used for a deeper understanding of the vibrational spectra of more complex nanoobjects—nanoheterostructures and quantum dots. In quantum dots, for example, the Raman lines may be associated with the breathing modes rather than LO phonons, because the most intensive lines in the spectra are usually the full-symmetry modes.

ACKNOWLEDGMENTS

The author is deeply grateful to R. B. Vasiliev for stimulating the author’s interest to nanoplatelets and fruitful discussions. This work was supported by the Russian Foundation for Basic Research (Grant No. 16-29-11694).

-
- [1] H. Lamb, *Proc. Roy. Soc. London A* **93**, 114 (1917).
 - [2] R. Fuchs and K. L. Kliewer, *Phys. Rev.* **140**, A2076 (1965).
 - [3] R. Ruppin and R. Englman, *Rep. Progr. Phys.* **33**, 149 (1970).
 - [4] S. Ithurria and B. Dubertret, *J. Am. Chem. Soc.* **130**, 16504 (2008).
 - [5] S. Ithurria, M. D. Tessier, B. Mahler, R. P. S. M. Lobo, B. Dubertret, and A. L. Efros, *Nat. Mater.* **10**, 936 (2011).
 - [6] J. Feldmann, G. Peter, E. O. Göbel, P. Dawson, K. Moore, C. Foxon, and R. J. Elliott, *Phys. Rev. Lett.* **59**, 2337 (1987).
 - [7] M. D. Tessier, C. Javaux, I. Maksimovic, V. Lorientte, and B. Dubertret, *ACS Nano* **6**, 6751 (2012).
 - [8] M. D. Tessier, B. Mahler, B. Nadal, H. Heuclin, S. Pedetti, and B. Dubertret, *Nano Lett.* **13**, 3321 (2013).
 - [9] A. W. Achtstein, A. Antanovich, A. Prudnikau, R. Scott, U. Woggon, and M. Artemyev, *J. Phys. Chem. C* **119**, 20156 (2015).
 - [10] Z. Chen, B. Nadal, B. Mahler, H. Aubin, and B. Dubertret, *Adv. Funct. Mater.* **24**, 295 (2014).
 - [11] F. Fan, P. Kanjanaboos, M. Saravanapavanantham, E. Beauregard, G. Ingram, E. Yassitepe, M. M. Adachi, O. Voznyy, A. K. Johnston, G. Walters, G.-H. Kim, Z.-H. Lu, and E. H. Sargent, *Nano Lett.* **15**, 4611 (2015).
 - [12] A. G. Vitukhnovsky, V. S. Lebedev, A. S. Selyukov, A. A. Vashchenko, R. B. Vasiliev, and M. S. Sokolikova, *Chem. Phys. Lett.* **619**, 185 (2015).
 - [13] J. Q. Grim, S. Christodoulou, F. Di Stasio, R. Krahn, R. Cingolani, L. Manna, and I. Moreels, *Nat. Nanotechnol.* **9**, 891 (2014).
 - [14] C. She, I. Fedin, D. S. Dolzhenkov, A. Demortière, R. D. Schaller, M. Pelton, and D. V. Talapin, *Nano Lett.* **14**, 2772 (2014).
 - [15] M. Li, M. Zhi, H. Zhu, W.-Y. Wu, Q.-H. Xu, M. H. Jhon, and Y. Chan, *Nat. Commun.* **6**, 8513 (2015).
 - [16] E. Lhuillier, J.-F. Dayen, D. O. Thomas, A. Robin, B. Doudin, and B. Dubertret, *Nano Lett.* **15**, 1736 (2015).
 - [17] S. A. Cherevkov, A. V. Baranov, A. V. Fedorov, A. P. Litvin, M. V. Artemyev, and A. V. Prudnikau, *Proc. SPIE* **8807**, 88070A (2013).
 - [18] S. A. Cherevkov, A. V. Fedorov, M. V. Artemyev, A. V. Prudnikau, and A. V. Baranov, *Phys. Rev. B* **88**, 041303 (2013).
 - [19] D. O. Sigle, J. T. Hugall, S. Ithurria, B. Dubertret, and J. J. Baumberg, *Phys. Rev. Lett.* **113**, 087402 (2014).

- [20] A. Girard, L. Saviot, S. Pedetti, M. D. Tessier, J. Margueritat, H. Gehan, B. Mahler, B. Dubertret, and A. Mermet, *Nanoscale* **8**, 13251 (2016).
- [21] V. Dzhagan, A. G. Milekhin, M. Y. Valakh, S. Pedetti, M. Tessier, B. Dubertret, and D. R. T. Zahn, *Nanoscale* **8**, 17204 (2016).
- [22] R. B. Vasiliev, A. I. Lebedev, E. P. Lazareva, N. N. Shlenskaya, V. B. Zaytsev, A. G. Vitukhnovsky, Y. Yao, and K. Sakoda, *Phys. Rev. B* **95**, 165414 (2017).
- [23] X. Gonze and C. Lee, *Phys. Rev. B* **55**, 10355 (1997).
- [24] M. Veithen, X. Gonze, and P. Ghosez, *Phys. Rev. B* **71**, 125107 (2005).
- [25] S. A. Prosandeev, U. Waghmare, I. Levin, and J. Maslar, *Phys. Rev. B* **71**, 214307 (2005).
- [26] To denote symmetric and antisymmetric Lamb modes, we use the notations a_i and s_i , where i indicates the order of the mode. The displacements of the atoms in these modes resemble the cosine function, with the $(i + 1/2)$ wave periods for symmetric modes and i full periods for antisymmetric modes.
- [27] In Lamb's original work, the waves in a thin plate were considered as purely acoustic waves in continuous media with zero-stress boundary conditions at the surfaces of the plate.
- [28] H. Fu, V. Ozoliņš, and A. Zunger, *Phys. Rev. B* **59**, 2881 (1999).
- [29] See Supplemental Material at <http://link.aps.org/supplemental/10.1103/PhysRevB.96.184306> for details and results of mode projection analysis and explanation of Raman lines intensity calculations.
- [30] To identify nanoplatelets, it is convenient to use the wavelength λ of the first exciton peak in their absorption spectra. The authors of Ref. [20] assumed the thickness to be 3 ML for nanoplatelets with $\lambda \approx 460$ nm, 4 ML for those with $\lambda \approx 515$ nm, and 5 ML for those with $\lambda \approx 550$ nm.
- [31] A. H. Nayfeh and P. B. Nagy, *J. Acoust. Soc. Am.* **101**, 2649 (1997).
- [32] Surface modes with frequencies intermediate between those of TO and LO phonons can be observed only on curved surfaces, in quantum dots and quantum wires.
- [33] As follows from the calculation of Raman spectra in biaxially compressed bulk CdSe, this energy shift can be explained by the in-plane compression of the modeled nanoplatelets, which decreases with increasing nanoplatelet thickness [22].
- [34] A. K. Arora, M. Rajalakshmi, T. R. Ravindran, and V. Sivasubramanian, *J. Raman Spectrosc.* **38**, 604 (2007).